

Disk Formation by AGB Winds in Dipole Magnetic Fields

Sean Matt and Bruce Balick

Astronomy Department, University of Washington, Seattle WA 98195;
matt@astro.washington.edu, balick@astro.washington.edu

and

Robert Winglee and Anthony Goodson

Geophysics Department, University of Washington, Seattle WA 98195;
winglee@geophys.washington.edu, anthony@geophys.washington.edu

ABSTRACT

We present a simple, robust mechanism by which an isolated star can produce an equatorial disk. The mechanism requires that the star have a simple dipole magnetic field on the surface and an isotropic wind acceleration mechanism. The wind couples to the field, stretching it until the field lines become mostly radial and oppositely directed above and below the magnetic equator, as occurs in the solar wind. The interaction between the wind plasma and magnetic field near the star produces a steady outflow in which magnetic forces direct plasma toward the equator, constructing a disk. In the context of a slow (10 km s^{-1}) outflow ($10^{-5} M_{\odot} \text{ yr}^{-1}$) from an AGB star, MHD simulations demonstrate that a dense equatorial disk will be produced for dipole field strengths of only a few Gauss on the surface of the star. A disk formed by this model can be dynamically important for the shaping of Planetary Nebulae.

Subject headings: MHD — planetary nebulae: general — stars: AGB and post-AGB
 — stars: magnetic fields — stars: winds, outflows

1. Introduction

Asymmetry presents one of the greatest challenges to our understanding of stellar outflows. Planetary nebulae (PNe) comprise a fairly well studied set of objects of which more than 80% are axisymmetric (Zuckerman & Aller 1986; Balick 1987; Stanghellini et al. 1993). Although the statistics for proto-PNe are limited (Sahai & Trauger 1998), the morphological statistics seen in PNe appear to apply. For this reason, and because they are generally bright and easily studied

observationally, PNe are an attractive set of objects to study if we are to gain insight into the physical mechanisms producing aspherical outflows.

In the past, the properties of PNe have been explained by an interacting stellar winds model (Kwok et al. 1978; Kahn & West 1985; Balick 1987). This holds that a fast, tenuous wind ($v \sim 1000$ km s⁻¹, $\dot{M} \sim 10^{-7} M_{\odot}$ yr⁻¹) from a PNe central star encounters an older, slower wind ($v \sim 10$ km s⁻¹, $\dot{M} \leq 0.1 M_{\odot}$ yr⁻¹). The slow material was expelled earlier ($\dot{M} \sim 10^{-5} M_{\odot}$ yr⁻¹), while the central star was on the asymptotic giant branch (AGB) or in the post-AGB phase. The shocked region between the two winds produces an expanding, wind-blown bubble (WBB) that is visible due to radiative cooling. To produce axisymmetric WBB's, the model assumes that the slow wind is aspherically distributed so that it is densest in the equatorial plane. Direct observational evidence for dynamically important disks, tori, and their remnants in the environment of PNe is clear at visible, infrared, and radio wavelengths (Huggins 2000; Meixner 2000; Balick 1987).

The central astronomical issue is how and why the slow winds can be equatorially concentrated. Physically, what processes are at work to build a disk? Winds from normal AGB and post-AGB stars are expected to be largely spherical, since the stellar surface is spherical and the wind driving force, radiation (Steffen et al. 1997; Habing et al. 1994), is isotropic. Thus, as the star evolves from the AGB into a white dwarf, the wind geometry is expected to remain symmetric.

However, as noted above, most PNe and proto-PNe show strong axisymmetries. Proposed mechanisms that might produce outflowing disks (see, e.g., Frank 1999 for a review) require reserves of angular momentum far in excess of that in the sun (Soker 1997). While some PNe may have formed from stars with companions close enough to transfer orbital angular momentum into the outer layers of a fully distended AGB star (Soker 1998a; Livio 1982), a mechanism that accounts for the nearly ubiquitous incidence of aspherical PNe is necessary. In addition, bipolar nebulae have a low galactic scale height and, consequently, are believed to evolve from relatively massive progenitors (Corradi & Schwarz 1995; Zuckerman & Gatley 1988). If so, a mechanism that produces stronger collimation exclusively around massive stars is needed.

Recently, several authors have discussed magnetic shaping mechanisms. Chevalier & Luo (1994) developed an analytical model in which a toroidal magnetic field carried in a fast wind produces prolate and bipolar WBB morphologies, even if the slow wind is spherically symmetric. Różyczka & Franco (1996), García-Segura (1997), and García-Segura et al. (1999) confirmed this model via numerical magnetohydrodynamic (MHD) simulations, demonstrating that toroidal magnetic fields carried in fast winds can constrain WBB outflow along the equator, producing a wide variety of polar flows. Their magnetic field topology is derived from what is expected in the solar wind, where the poloidal field lines connecting the outflowing wind to the solar surface are wound up due to the rotation of the sun. However, these and other (Pascoli 1992; Pascoli et al. 1992) models have only considered the effect of toroidal magnetic fields. The influence of *poloidal* magnetic fields on AGB winds is yet unexplored.

The sun has poloidal magnetic field that is dynamically important to the solar wind, as ev-

idenced by streamers and coronal mass ejections. In fact, the sun’s magnetic field is dominated by the (global) dipole component outside a few solar radii throughout most of the magnetic cycle (Bravo et al. 1998). Several authors (Mestel 1968; Pneuman & Kopp 1971; Washimi et al. 1987; Mestel & Spruit 1987; Washimi 1990; Washimi & Shibata 1993; Banaszekiewicz et al. 1998; Keppens & Goedbloed 1999, 2000) have shown that the dipole field has a significant influence on the solar wind. Washimi et al. (1987) and Keppens & Goedbloed (1999) reported an equatorial density enhancement in the solar wind, due to the poloidal field (in the absence of rotation). It therefore may be insufficient to consider the effects of toroidal magnetic fields alone on stellar winds without including the effects of the poloidal fields.

Our main goal is to show that a simple poloidal magnetic field, a dipole, can be dynamically important in stellar winds. We propose and justify a simple mechanism that might form strongly axisymmetric winds in isolated AGB or post-AGB stars without the need for large amounts of rotation. In the presence of a dipole field, wind plasma is deflected toward the equator, and a disk can be produced. We detail the qualitative aspects of the model in §2 and present numerical magnetohydrodynamic (MHD) simulations that confirm the conceptual model in §3. A discussion of some of the implications of this work is included in §4.

2. The Conceptual Model

Consider a wind from a spherical star. In the absence of rotation and magnetic fields, the launching of the wind is completely isotropic if the wind is driven by radiation pressure on dust or thermal pressure. The wind accelerates to a terminal velocity within several stellar radii (Lamers & Cassinelli 1999). However, if the star initially has a dipole magnetic field on the surface, we demonstrate that the end result is an outflow that is densest in the magnetic equatorial plane.

For this to occur, the wind must be sufficiently ionized so that the magnetic field is frozen into the plasma. If the total (thermal plus kinetic) energy of the wind is much greater than the magnetic energy, the magnetic field is carried radially outward in the wind. The magnetic field topology becomes radial everywhere. The field direction is inherited from the dipole in that the field lines are oppositely directed above and below the equator. This can be understood if one considers one end of each field line to be “anchored” to the surface of the star while the other end is stretched radially outward in the wind. In this case (very weak field), the wind will be isotropic. Figure 1 illustrates the approximate topology of a weak magnetic field. In order to maintain a radial magnetic field (with an equatorial direction reversal), an azimuthally directed current sheet must exist in the equatorial plane. As shown in Figure 1, the resulting magnetic force ($\mathbf{J} \times \mathbf{B}$, where \mathbf{J} is the volume current and \mathbf{B} the magnetic field) is directed toward the equator.

If the magnetic field energy on the surface of the star is comparable to or greater than the energy in the wind, this $\mathbf{J} \times \mathbf{B}$ force will be strong enough to redirect the wind. In other words, plasma will be forced to flow along the dipole field lines near the star. Since the plasma is frozen-in

to the magnetic field, continuity requires that the wind momentum is proportional to r^{-3} , since $\mathbf{B} \propto r^{-3}$ for a dipole. For an accelerating wind, the kinetic energy will therefore decrease more slowly than r^{-3} , while the dipole magnetic energy decreases as r^{-6} . Hence, the magnetic field is only effective near the star. So no matter how strong the field is, there will always be an exterior region of the outflow that is dominated by the kinetic energy of the wind (and where the field lines become radial). Numerical simulations presented in §3.3 and done by others (Pneuman & Kopp 1971; Washimi & Shibata 1993; Keppens & Goedbloed 1999, 2000) confirm this idea.

For very strong magnetic fields, the wind may be completely quenched near the equator (Keppens & Goedbloed 2000). In this case the low-latitude magnetic field lines remain closed (each end attached to the star at equal but opposite latitudes, forming a static loop), and no ionized particles can flow from this region (ignoring diffusive effects). However, the high-latitude magnetic field lines would still open (tending toward radial at large radii), but the plasma leaving at these high latitudes will first be forced toward the equator (Pneuman & Kopp 1971; Washimi et al. 1987; Keppens & Goedbloed 1999).

The two insets in Figure 1 show the approximate magnetic field topology in the wind near a star with a moderate (magnetic and wind energy comparable) and strong (magnetic energy dominates) initial dipole magnetic field. As shown, plasma flowing along open field lines is first directed more toward the equator than radial lines and eventually tend toward radial. The net effect of this flow pattern is an increase of the wind density and thermal pressure near the equator, and a decrease near the poles. This is similar to what happens in solar coronal streamers. Open streamers have all open field lines, helmet streamers have some closed loops, and both types show density enhancements along radial lines through their centers. The model presented here can superficially be thought of as a star with an axisymmetric, global streamer encircling its equator, thus forming a disk. It is this concept that we propose may be responsible for forming outflowing disks from AGB or post-AGB stars.

In addition to having a density anisotropy, the redistribution of gas pressure can affect, via ∇P forces, the radial force on the wind such that the wind on the equator is accelerated more slowly than the wind on the poles. This leads to a wind that is slowest near the equator. In many astrophysical winds, gas pressure gradients are negligible, and so the wind velocity may be unaffected by this. Such winds, however, would still be deflected toward the equator as discussed above.

It is instructive to note that the strength of a dipole magnetic field falls off as r^{-3} , while a radial field goes as r^{-2} . This means that there is more total magnetic energy in the radial field than in the dipole field. This energy is added by the wind as it does work to stretch out the field lines. In other words, no magnetic flux is carried off of the surface of the star (once the wind is established), though the stretched field remains anchored on the star, and the axisymmetric density distribution remains intact. This is because the $\mathbf{J} \times \mathbf{B}$ forces balance the gas and dynamic pressure gradient forces, and the plasma flow is parallel to the magnetic field. Hence, the star does

not need to continue to produce any new magnetic energy (after the initial dipole is produced), provided the diffusion timescale is significantly longer than the dynamical timescale of the outflow. However, observations of PNe progenitors and central stars show that the wind speed increases from $\sim 10 \text{ km s}^{-1}$ to $\sim 1000 \text{ km s}^{-1}$ as the star evolves while \dot{M} decreases from $\sim 10^{-4} M_{\odot} \text{ yr}^{-1}$ to $\sim 10^{-8} M_{\odot} \text{ yr}^{-1}$ (Frank 1999). The stellar surface temperature, radius, gravity, and luminosity all evolve rapidly. It is therefore plausible that the magnetic field is only of transient importance in structuring the wind geometry of these stars.

3. MHD Simulations

Here we present numerical MHD simulations testing this model in the context of winds from the surface of an AGB star. The simulations are simplified in that they do not include the effects of rotation, gravity, or radiative cooling, they are carried out in two dimensions, and the wind is driven radially by thermal pressure at the star’s surface. They are meant to serve only as a demonstration of feasibility for the MHD model, and to investigate the types of results that can be expected for more sophisticated computational models.

We have neglected rotation to study winds from isolated stars (that is, they are not spun-up). A giant star with solar angular momentum is expected to rotate very slowly relative to its breakup velocity (Pascoli 1987; Soker 1997). Presumably, a star must have some amount of rotation in order to generate a magnetic field, via a stellar dynamo (Parker 1979), but if the rotation velocity on the surface is much less than the outflow velocity of the wind, we assume that rotational influence on the isotropy of the wind is negligible.

A more realistic treatment would include the effects of gravity. This would affect the details of the acceleration of the wind, but would not change the results of the qualitative model. The simulations presented here are most applicable to stars in which the radiation pressure balances gravity above the surface so that only pressure and magnetic forces are important. We want to stress, however, that the model is not dependent on the wind driving mechanism.

Below, we discuss the code and boundary conditions (§3.1), initial conditions (§3.2), and simulation results for various magnetic field strengths (§3.3).

3.1. Simulation Code

The simulation code uses a two-step Lax-Wendroff (finite difference) scheme (Richtmyer & Morton 1967) to simultaneously solve the single-fluid, ideal MHD equations

$$\frac{\partial \rho}{\partial t} = -\nabla \cdot (\rho \mathbf{v}) \tag{1}$$

$$\frac{\partial(\rho \mathbf{v})}{\partial t} = -\nabla(\rho v^2 + P) + \frac{1}{c}(\mathbf{J} \times \mathbf{B}) \tag{2}$$

$$\frac{\partial e}{\partial t} = -\nabla \cdot [\mathbf{v}(e + P)] + \mathbf{J} \cdot \mathbf{E} \quad (3)$$

$$\frac{\partial \mathbf{B}}{\partial t} = -c(\nabla \times \mathbf{E}) \quad (4)$$

in two dimensions, and uses

$$\mathbf{E} = -\frac{1}{c}(\mathbf{v} \times \mathbf{B}) \quad (5)$$

$$\mathbf{J} = \frac{c}{4\pi}(\nabla \times \mathbf{B}) \quad (6)$$

$$e = \frac{1}{2}\rho\mathbf{v}^2 + \frac{P}{\gamma - 1} \quad (7)$$

where ρ is the density, \mathbf{v} the velocity, P the scalar gas pressure, e the internal energy density, \mathbf{B} the magnetic field, \mathbf{J} the volume current, \mathbf{E} the electric field, c the speed of light, and γ the ratio of specific heats (we used $\gamma = 1.4$ in our simulations).

We employ a three-layer boundary condition at the base of the wind to avoid complications introduced by the finite-difference scheme that numerically violate $\nabla \cdot \mathbf{B} = 0$ near fixed boundaries. On the innermost boundary, all plasma quantities (P , ρ , \mathbf{v}) are constant (in time) and \mathbf{B} is held at the dipole value. The intermediate boundary is the same as the inner boundary except that \mathbf{B} is time-dependent. The outer boundary is the same as the inner boundary except that both \mathbf{B} and \mathbf{v} are time-dependent. We consider the intermediate boundary to be the “surface” of the star, though the density and pressure are constant on the outer-most layer. These boundary conditions allow the magnetic field on the stellar surface to be carried outward in the wind in a manner that preserves $\nabla \cdot \mathbf{B} = 0$. Outside the star, all quantities are time-dependent. The large-scale results are not sensitive to the details of these boundary conditions.

The simulations use a 500×500 point Cartesian grid and a “star” with a radius of six gridpoints at the center. If we assume the star has a radius of $R_* = 1.5 \times 10^{13}$ cm, this corresponds to a total “field of view” of 83×83 AU with a “resolution” of $1/6$ AU. The calculations are strictly 2-D, and no symmetry constraint is imposed.

The 2-D dipole equation is given in polar coordinates as

$$\begin{aligned} B_r &= M \left(\frac{R_*}{r} \right)^2 \cos \theta \\ B_\theta &= M \left(\frac{R_*}{r} \right)^2 \sin \theta \end{aligned} \quad (8)$$

where M is the field strength at the surface, R_* is the radius of the object, and θ is the angle from the magnetic pole. This field satisfies $\nabla \cdot \mathbf{B} = 0$ and $\nabla \times \mathbf{B} = 0$ (the dipole is current-free) in two dimensions. It is different from a 3-D dipole in that the field strength at the poles is equal to (instead of twice) that at the equator, and the 2-D dipole falls off as r^{-2} (instead of r^{-3}).

3.2. Initial Conditions

While these simulations apply to a family of systems (i.e. they are scalable), we report numerical parameters and results for a system in which the star has a radius of 1 AU. If the physical values of \mathbf{v} , ρ , P , and \mathbf{B} remain unchanged, the results apply to a star of arbitrary radius, distances and times scale with R_* , and \dot{M} with R_*^2 . In this way, we can superficially consider outflow from an AGB and post-AGB star simultaneously.

Before the simulations begin, the star has a constant density of $n = 3.4 \times 10^{11} \text{ cm}^{-3}$ and a pressure such that the sound speed is 5.9 km s^{-1} on its three-layer boundary. These conditions lead to a mass flux and outflow velocity (see §3.3) that are reasonable for a wind from a cool AGB star. The star also has a dipole magnetic field (Eqn. 8) initialized everywhere in the simulation region. The velocity of the plasma is initially zero everywhere.

When the simulation begins, the difference between the stellar surface pressure and that of the surrounding ambient material leads to an outward acceleration of gas, which plows the ambient material ahead of it. After the ambient gas is completely swept off of the simulation grid, a steady-state outflow is established whose properties only depend on the conditions on the surface of the star. In fact, provided that the outflow becomes supersonic, the results are insensitive to the initial conditions of the ambient gas. Since we were only interested in the characteristics of the steady-state outflow, we chose the density and sound speed of the ambient gas ($1.0 \times 10^9 \text{ cm}^{-3}$ and 11.8 km s^{-1} , respectively) so that it is efficiently cleared out of the simulation region. It should be noted that the steady state of the outflow is due to the unchanging (in time) boundary conditions on the surface of the star. On real stars, dynamic surface processes and stellar evolution require that winds are time-dependent (on long enough timescales). We are, however, only currently interested in determining the properties of the wind while the star satisfies the conditions outlined above.

In order to determine whether the magnetic field might influence the wind, one can use the ratio of the wind energy density to the magnetic energy density. This ratio increases with distance from the star (see §2), so the magnetic field will be most effective near the surface. If the wind has a constant energy from the stellar surface outward, this ratio on the surface ($r = 0$) is given by $\dot{M}v_f R_*^{-2} B_0^{-2}$, assuming that thermal pressure is negligible far from the star and where v_f is the terminal velocity of the wind. If energy is added to the wind above the surface (e.g., via radiation pressure or magnetic effects), this is an upper limit.

This formula for the ratio of wind to magnetic energy is convenient because it gives the relative importance of a hypothetical or measured magnetic field using measured wind parameters. By setting it equal to unity, one obtains (roughly) a minimum magnetic field strength capable of deflecting the stellar wind. Note that this formula determines *whether* the magnetic field is important, while the topology of the field determines *how* the wind is affected. For an AGB star with $\dot{M} \sim 10^{-5} M_\odot \text{ yr}^{-1}$, $v_f \sim 10 \text{ km s}^{-1}$, and $R_* \sim 1.5 \times 10^{13} \text{ cm}$, this implies that the wind and magnetic energy densities are comparable for a magnetic field strength of 1.7 Gauss on the surface. For this reason, we ran seven different simulations with surface magnetic field strengths bracketing

this value.

In the simulations, the outflow is pressure-driven, so the total energy in the wind as it accelerates outward is equal to its thermal energy on the surface (where $\mathbf{v} = 0$). For the simulations, then, the key parameter (the ratio of wind to magnetic energy densities) is simply

$$\beta = \frac{8\pi P_0}{\mathbf{B}_0^2} = \frac{\text{thermal energy}}{\text{magnetic energy}} \quad (9)$$

where the subscript 0 denotes quantities initially on the stellar surface. In all of the simulations, the initial gas properties are constant and only the strength of the magnetic field varies.

3.3. Simulation Results

The simulations comprise seven different cases spanning $\beta = \infty$ to 0.1, corresponding to $\mathbf{B}_0 = 0$ and 6.0 Gauss on the surface of the star, respectively. The first two columns of Table 1 list the values of β for all cases and the corresponding dipole magnetic field strength initially on the surface of the star.

The $\beta = \infty$ case is mainly used as a reference to which we compare the cases that include magnetic fields. Figure 2 shows the density and velocity profile of this non-magnetic case in steady-state. The wind accelerates to $\sim 11 \text{ km s}^{-1}$ within $10R_*$ (becoming supersonic) and increases very little as it travels further from the star. Using the density and velocity just outside the surface of the star, the calculated 2-D mass flux is $2.8 \times 10^{-6} \text{ M}_\odot \text{ yr}^{-1} \text{ AU}^{-1}$ ($= 2\pi\rho\mathbf{v}r$) for pure hydrogen. This quantity is the mass flux per length normal to the 2-D plane. The equivalent mass flux for a 3-D system would be $\dot{M} = 5.6 \times 10^{-6} \text{ M}_\odot \text{ yr}^{-1}$, assuming the star is spherical. The velocity and mass flux of this outflow are consistent with assumed properties in the winds of AGB stars (Frank 1999).

All of the cases established steady-state outflows in the entire simulation region in less than 200 years, comparable to the time needed to clear out the initial ambient gas. Figure 3 shows the magnetic field lines and gas pressure contours overplotting a grey-scale image of the current density for the case with $\beta = 0.2$. A comparison with Figure 1 indicates a confirmation of the qualitative model (§2). The current and magnetic field lines in the simulation are oriented in the same direction as predicted by the model. The pressure gradient is significantly anisotropic such that it is steeper on the poles than on the equator (near the star), as expected.

An interesting feature of Figure 3 is that the magnetic field lines are not perfectly radial. Far from the star, the lines tend toward radial, but near the star, they are directed more toward the equator than radial lines. This result is expected since, in this case, the magnetic energy is greater than the wind energy on the stellar surface (see §2). The dependence of magnetic field topology on field strength is even more apparent in Figure 4, which shows the density and field lines for the $\beta = 5.0$ and 0.1 cases. The lines are almost completely radial in the weak field case (left panel),

while for the stronger field (right panel), they retain much of their original (dipole) structure near the star. A comparison of Figures 4 and 1 suggests that our simulation with the strongest magnetic field should still be considered to have a “moderate” field strength, since there are no large closed field lines. Since the flows are in steady-state, the magnetic field lines are in the same direction as streamlines for wind particles. With this in mind, it is easier to understand the equatorial density enhancement visible in the right panel of Figure 4.

Figure 5 shows the density distribution in the outflow for six cases. As β decreases, the density contours become less circular, having a major axis along the equator and a minor axis along the poles. This indicates a correlation between the equatorial concentration of the wind and the magnetic field strength. For the weak-field cases ($\beta > 1$, top row of Fig. 5), the density contours are only slightly different (by a few tenths or less) from circles. For smaller β , however, the magnetic field has a stronger influence on the outflow properties, and the density contours are much more disk-like.

This trend is more apparent in the left panel of Figure 6, a plot of density as a function of latitude at $3.3R_*$ for all cases. The non-magnetic case (thick line) is isotropic, but for decreasing β , the outflow is denser near the equator and more tenuous near the poles. This illustrates that the wind plasma at high latitudes is moved toward lower latitudes by magnetic forces. For $\beta \leq 1.0$, steep density profiles indicate the presence of an outflowing disk that is fed by high latitude material. For the $\beta = 0.1$ and 0.2 cases, the flatness of the disk is unresolved on the simulation grid near the star. This is evident in the left panel of Figure 6, as these two density profiles display a sharp point (cusp) at the equator. A velocity trend is evident in the right panel of Figure 6 where the wind speed is shown as a function of latitude at a radius of $3.3R_*$. Here, it is evident that the wind is slower near the equator and faster near the poles for decreasing β .

The outflow in the non-magnetic case deviates slightly from purely isotropic due to grid orientation effects that arise from placing a round star in a Cartesian grid, coupled with difficulties of the numerical scheme on the “stair-step” corners of the gridded stellar surface. This is apparent in the upper left panel of Figure 5 and the thick line in both panels of Figure 6. The very slight anisotropy of the non-magnetic outflow represents an uncertainty in the results for all cases, due to these gridding effects. At any radius, the outflow properties (ρ , \mathbf{v} , P) of the non-magnetic case vary by less than 10%. It is also important to note that the outflow properties on the poles of the non-magnetic flow are identical to those on the equator.

The equator-to-pole density ratio, q (the “density contrast”), is a useful way to characterize the axisymmetric inertial properties of the wind. Figure 7 shows the density contrast as a function of distance from the star. The correlation between q and magnetic field strength is valid for all radii, though q is not constant everywhere. For the cases with $\beta \leq 1.0$, q reaches a maximum inside $r = 5R_*$, then decreases for increasing r . This can be understood if we note that the magnetic energy becomes much weaker than total wind energy outside a few stellar radii for all cases. When q is large, there are pressure gradients directed away from the equator (i.e., the disk is compressed

by the field, evident in Fig. 3). As the wind moves outward to the region where the wind energy dominates, it can expand away from the equator, causing a decrease in q (the densities in Fig. 6 are plotted near where the maximum contrast occurs in all cases). Here, of course, we have ignored radiative cooling in the disk, which may be unrealistic.

The last two columns of Table 1 summarize the simulation results of Figure 7. The maximum value of q for each β and the values at $40R_*$ are listed. For the $\beta = 0.1$ and 0.2 cases, we can only place lower limits on the maximum q because the resulting disk is unresolved in our simulations near the star (as discussed above).

In general, density contrasts of roughly less than 2 in the slow AGB wind may lead to elliptical PNe, while larger contrasts probably produce bipolars (Frank 1999). However, the density contrast is not solely responsible for determining the shape of PNe, and the distribution of mass is also important. In order to superficially test the inertial properties of the slow outflows produced in our simulations, we ran another simulation that included a fast wind. For the initial conditions of this simulation, we used the end result of the $\beta = 0.5$ simulation (see the bottom middle panel of Fig. 5). We then adjusted the pressure (increased by a factor of 10) and density (decreased by a factor of 1000) on the surface of the star so that a fast ($v \sim 1000 \text{ km s}^{-1}$), tenuous ($\dot{M} \sim 6 \times 10^{-7} M_{\odot} \text{ yr}^{-1}$) wind blew from the star and collided with the slow-moving disk, producing a shocked, wind-blown bubble. On the surface of the fast wind producing star, $\beta = 5.0$, so the fast wind is affected very little by the magnetic field on the surface. Figure 8 shows the density and velocity vectors on the simulation grid 2 years after the onset of the fast wind. The darkest region in the figure corresponds to shocked, slow-wind material that has been swept up in the fast wind. While this simulation is too simple (e.g., radiative cooling is ignored) to compare to real objects, Figure 8 demonstrates that disks formed by outflows from stars with dipole fields can be dynamically important for shaping PNe.

4. Discussion

We have presented a simple mechanism for producing an equatorially concentrated wind from an isolated star. The wind is isotropic in the absence of magnetic effects. In the presence of a dipole magnetic field, however, the self-consistent interaction between the wind plasma and the magnetic field causes the wind to become denser along the magnetic equator and less dense near the poles. The outflow model is valid for very slowly rotating stars. In fact, the model itself requires no rotation, other than that necessary for generating the magnetic field.

In the steady-state, the magnetic field retains much of its dipole shape near the star, but becomes mostly radial outside a few stellar radii and is oppositely directed above and below the magnetic equator. This resembles the magnetic field configuration expected in the solar wind (Altschuler & Newkirk 1969; Washimi & Shibata 1993; Parks 1991) with two major exceptions: 1) Solar rotation adds an azimuthal (toroidal) component to otherwise radial field lines, and 2) higher-

order (though only important very near the sun) and time-dependent magnetic fields (Bravo et al. 1998) are important on the sun and further complicate the magnetic structure.

Our MHD simulations suggest that large equator-to-pole density contrasts can be produced near an AGB star with a dipole magnetic field strength of only a few Gauss on the surface. Stronger fields produce larger contrasts. In addition to being denser, the wind near the star is somewhat slower on the equator than along the poles.

As a simple test of validity, this model can be applied to the sun. If we apply the argument given in §3.2 to the solar wind ($\dot{M} \sim 10^{-13} M_{\odot}\text{yr}^{-1}$, $v_f \sim 400 \text{ km s}^{-1}$, $R_{\odot} \sim 7 \times 10^{10} \text{ cm}$), we find that the wind and magnetic energy densities are comparable for a magnetic field strength of 0.23 Gauss on the surface of the sun. This implies that the global average dipole field on the sun (often 1-2 Gauss) may have a significant effect on the isotropy of the solar wind via the mechanism discussed here. This is not surprising. Mestel (1968) and Pneuman & Kopp (1971), for example, demonstrated that the solar dipole is strong enough to retain closed field loops (see §2) in the equatorial region. The models of Washimi et al. (1987) and Keppens & Goedbloed (1999) indicated that such a field can lead to an equatorial density enhancement in the solar wind. On the observational front, Ulysses measurements (Goldstein et al. 1996) indicate the solar wind is denser within 20 degrees of the solar equator than at high latitudes by a factor of roughly 2. We should note that the solar wind is very complex, and the equatorial density enhancement in the solar wind may have other or multiple origins.

According to the currently popular paradigm (Balick 1987), PNe may be the result of a fast stellar wind colliding with a slower, denser wind, producing an expanding shock front. If the slow wind is produced by the mechanism presented here, it will be denser and slower in the equatorial plane. These properties define an aspherical inertial barrier (a nozzle) that would allow the PN to expand more freely along the poles. The extremity of this effect varies with the strength of the star’s dipole magnetic field while it is near the end of its slow wind-producing phase. Spherical PNe should result from stars that had fields weaker than ~ 0.5 Gauss on the surface, while stronger fields might lead to elliptical and bipolar PNe shapes.

We propose that sometime prior to the formation of the bright cores of PNe, dipole magnetic fields are generated (via a dynamo) or exposed (as winds remove the outer layers) on the surface of the star. The wind and field construct a toroidal circumstellar environment (or outflowing disk) as described above. Even if the subsequent fast winds become isotropic, this disk can collimate the outflow until instabilities or ablation destroy the disk. We shall explore this further in subsequent papers. If the magnetic field is systematically stronger for more massive stars, the observed correlation between bipolarity and large progenitor mass (Zuckerman & Gatley 1988; Corradi & Schwarz 1995) is nicely explained.

The development of the disk is essentially instantaneous with the emergence of the magnetic field. Thus, if the magnetic field were to appear abruptly, one might expect mass loss to be initially isotropic in character, followed by an abrupt change in geometry. There is observational evidence

for such a “mode change” in AGB winds for several objects (Hajian et al. 1997; Terzian & Hajian 2000; Balick & Wilson 2000). How such a change in the magnetic field could occur in an AGB star is outside the scope of this paper, since it implies a significant evolutionary change in the star.

The simplicity of the mechanism presented here makes it appealing, but real stars are much more complicated. More work is necessary to apply the model to real stars. For example, AGB winds are not likely to be primarily pressure-driven as we have considered here. A more realistic treatment of the model should include the influence of radiation pressure on dust grains (Habing et al. 1994; Steffen et al. 1997), radiative cooling, simulations in 3-D, the effects of higher-order magnetic fields and fields with other symmetries (e.g. toroidal fields produced by a dynamo or rotation), and the effects of stellar rotation (Bjorkman & Cassinelli 1993; Washimi & Shibata 1993). Also, the fact that our model reaches a steady-state results from our assumption that the surface properties do not change. In real AGB stars, pulsations may affect the wind (though if they are isotropic, they can’t effect the isotropy of the flow). In the presence of magnetic fields, convection and differential rotation probably leads to more dynamic processes such as flares, coronal mass ejections, spots (Frank 1995; Soker 1998b), magnetic cycles (Soker 2000), etc., as occur on the sun.

In winds where pressure gradient forces are less important (e.g., for radiation pressure-driven or radiatively cooled winds), the outflow should behave differently. For example, in our adiabatic simulations the density contrast in the wind reached a peak and then decreased in value further from the star (see Fig. 7). This is probably due to pressure gradient forces directed away from the equator (see Fig. 3). If these forces are small, the disk material may not expand as much (the disk will remain flatter), leading to larger density contrasts than reported here.

While a more realistic approach than we have taken will affect the details of the outflow, the qualitative model should apply to all stars that have dipole magnetic fields of moderate strength (magnetic energy comparable to the wind energy near the surface).

The authors would like to thank Adam Frank, Andrew Markiel, and Stacy Palen for insightful discussion of many aspects of this work. We are also grateful to the referee, whose detailed comments led to significant improvement of the paper. This research was supported by NSF grant AST-9729096.

REFERENCES

- Altschuler, M. D., & Newkirk, G. 1969, *Sol. Phys.*, 9, 131
- Balick, B. 1987, *AJ*, 94, 671
- Balick, B., & Wilson, J. M. 2000, *BAAS*, 196, #44.01
- Banaszkiewicz, M., Axford, W. I., & McKenzie, J. F. 1998, *A&A*, 337, 940

- Bjorkman, J. E., & Cassinelli, J. P. 1993, *ApJ*, 409, 429
- Bravo, S., Stewart, G. A., & Blanco-Cano, X. 1998, *Sol. Phys.*, 179, 223
- Chevalier, R., & Luo, D. 1994, *ApJ*, 421, 225
- Corradi, R. L. M., & Schwarz, H. E. 1995, *A&A*, 293, 871
- Frank, A., 1995, *AJ*, 110, 2457
- Frank, A., 1999, *New Astronomy Reviews*, 43, 31
- García-Segura, G. 1997, *ApJ*, 489, L189
- García-Segura, G., Langer, N., Różycka, M., and Franco, J. 1999, *ApJ*, 517, 767
- Goldstein, B., Neugebauer, M., Phillips, J., Bame, S., Gosling, J., McComas, D., Wang, Y.-M., Sheeley, N., & Seuss, S. 1996, *A&A*, 316, 296
- Habing, H. J., Tignon, J., & Tielens, A. G. G. M. 1994, *A&A*, 286, 523
- Hajian, A., Frank, A., Balick, B., & Terzian, Y. 1997, *ApJ*, 477, 226
- Huggins, P. J. 2000, in *ASP Conf. Ser. 199, Asymmetrical Planetary Nebulae II: From Origins to Microstructures*, ed. J. H. Kastner, N. Soker, & S. Rappaport, 277
- Kahn, F., & West, K. 1985, *MNRAS*, 212, 837
- Keppens, R., & Goedbloed, J. P. 1999, *A&A*, 343, 251
- Keppens, R., & Goedbloed, J. P. 2000, *ApJ*, 530, 1036
- Kwok, S., Purton, C. R., & FitzGerald, P. M. 1978, *ApJ*, 219, L125
- Lamers, H. J. G. L. M., & Cassinelli, J. P. 1999, *Introduction to Stellar Winds* (NY: Cambridge Univ. Press)
- Livio, M. 1982, *A&A*, 105, 37
- Meixner, M. 2000, in *ASP Conf. Ser. 199, Asymmetrical Planetary Nebulae II: From Origins to Microstructures*, ed. J. H. Kastner, N. Soker, & S. Rappaport, 135
- Mestel, L. 1968, *MNRAS*, 138, 359
- Mestel, L., & Spruit, H. C. 1987, *MNRAS*, 226, 57
- Parker, E. N. 1979, *Cosmical Magnetic Fields* (Oxford: Clarendon)
- Parks, G. K. 1991, *Physics of Space Plasmas: An Introduction* (New York: Addison-Wesley)

- Pascoli, G. 1987, *A&A*, 180, 191
- Pascoli, G. 1992, *PASP*, 104, 350
- Pascoli, G., Leclercq, J., & Poulain, B. 1992, *PASP*, 104, 182
- Pneuman, G. W., & Kopp, R. A. 1971, *Sol. Phys.*, 18, 258
- Richtmyer, R. D., & Morton, K. W. 1967, *Difference Methods for Initial-Value Problems* (New York: Wiley-Interscience)
- Róższycza, M., & Franco, J. 1996, *ApJ*, 469, L127
- Sahai, R., & Trauger, J. 1998, *ApJ*, 116, 1357
- Soker, N. 1997, *ApJS*, 112, 487
- Soker, N. 1998a, in *ASP Conf. Ser. 154, The 10th Cambridge Workshop on Cool Stars, Stellar Systems and the Sun*, ed. R. A. Donahue & J. A. Bookbinder, 1901
- Soker, N. 1998b, *MNRAS*, 299, 1242
- Soker, N. 2000, *ApJ*, in press
- Stanghellini, L., Corradi, R. L. M., & Schwarz, H. E. 1993, *A&A*, 279, 521
- Steffen, M., Szczerba, R., Men'shchikov, A., & Schönberner, D. 1997, *ApJS*, 126, 39
- Terzian, Y., & Hajian, A. R. 2000, in *ASP Conf. Ser. 199, Asymmetrical Planetary Nebulae II: From Origins to Microstructures*, ed. J. H. Kastner, N. Soker, & S. Rappaport, 33
- Washimi, H., Yoshino, Y., & Ogino, T. 1987, *Geophys. Res. Lett.*, 14, 487
- Washimi, H. 1990, *Geophys. Res. Lett.*, 17, 33
- Washimi, H., & Shibata, S. 1993, *MNRAS*, 262, 936
- Zuckerman, B., & Aller, L. H. 1986, *ApJ*, 301, 772
- Zuckerman, B., & Gatley, I. 1988, *ApJ*, 324, 501

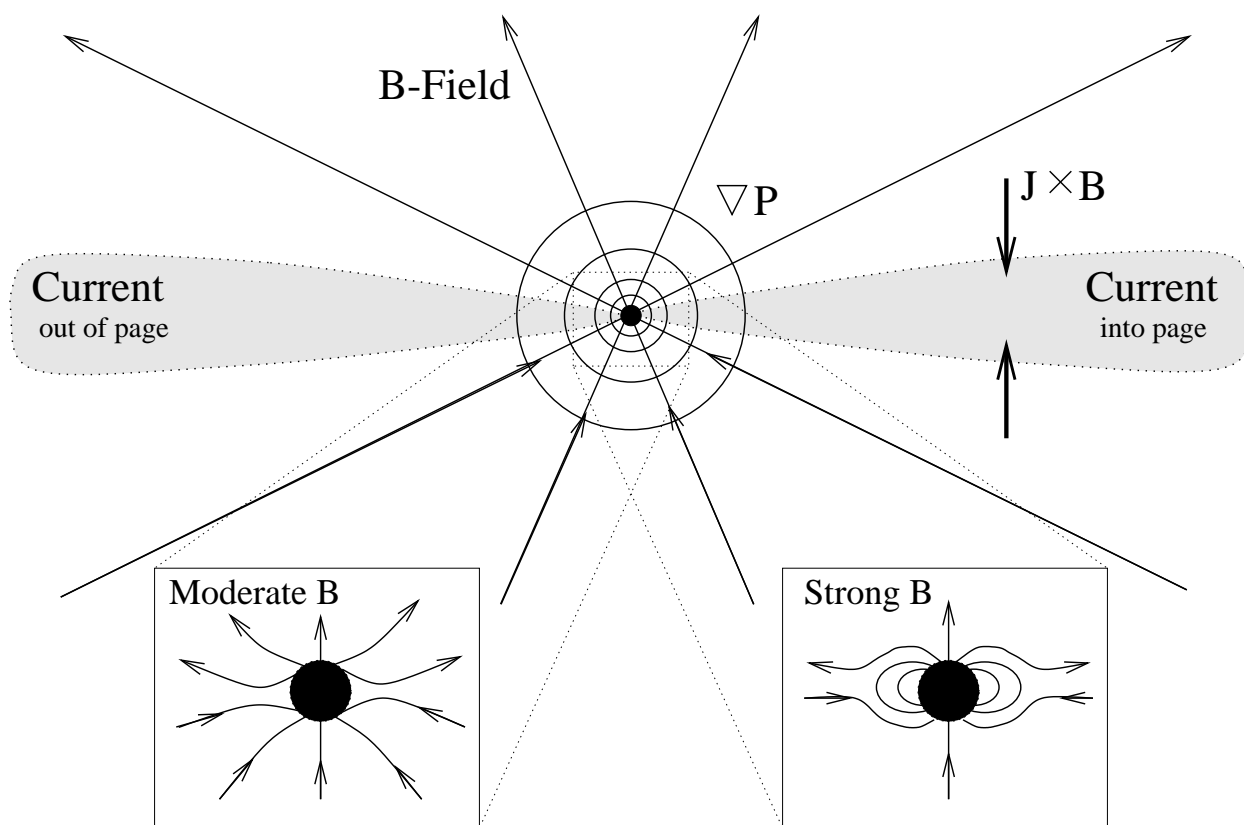


Fig. 1.— A qualitative cartoon of the model including magnetic field lines and pressure contours is shown. In steady-state, a weak, initially dipolar magnetic field (\mathbf{B}) becomes radial but oppositely directed above and below the magnetic equator, and a wind is driven isotropically from the surface of the star. An equatorial current sheet (\mathbf{J}) exists to maintain the radial magnetic field. The resulting ($\mathbf{J} \times \mathbf{B}$) force is directed toward the equator. For moderate (left inset) or strong (right inset) dipole magnetic fields, the magnetic force is sufficient to divert the wind toward the equator.

Table 1. Simulation Results

β	B_0 (Gauss)	q (max)	q ($40R_*$)
0.1	5.97	> 5.4	2.8
0.2	4.22	> 4.3	2.5
0.5	2.67	2.8	2.2
1.0	1.89	2.1	1.8
2.0	1.34	1.5	1.4
5.0	0.84	1.2	1.2
∞	0.00	1.0	1.0

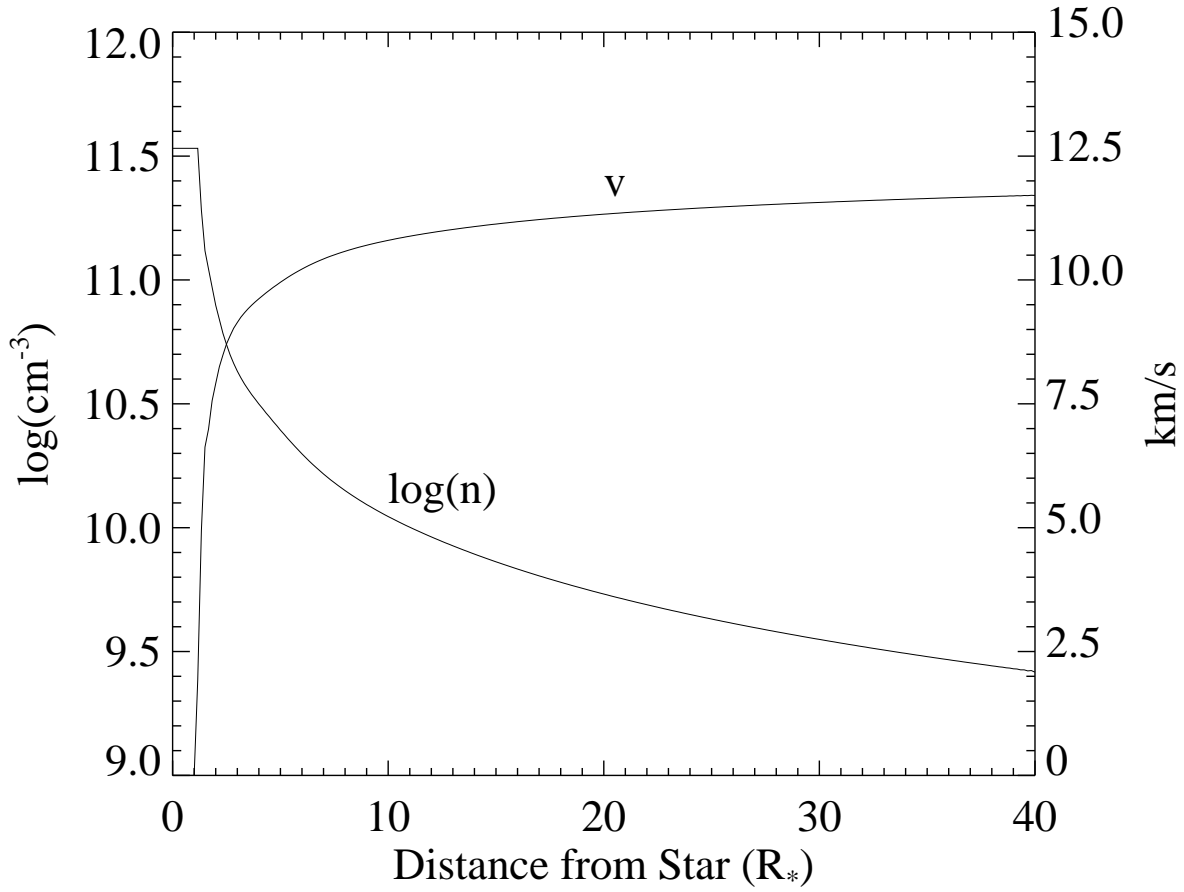


Fig. 2.— The isotropic wind density and velocity as a function of distance from the star is shown for the steady-state, non-magnetic outflow.

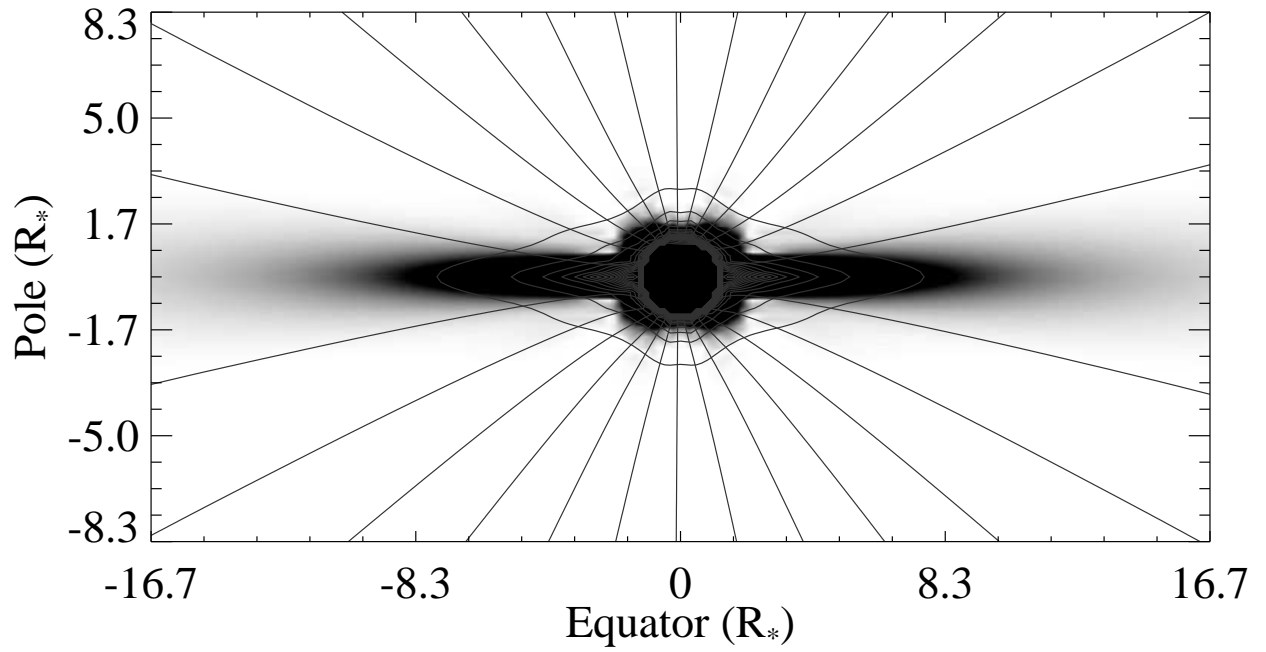


Fig. 3.— Shown is an image of the absolute value of the azimuthal current density for the $\beta = 0.2$ case after it has reached steady-state. Only the inner 200×100 grid points are shown. Black corresponds to $\mathbf{J} \geq 1.5 \times 10^{-4} \mu\text{A m}^{-2}$ while $\mathbf{J} \leq 7.3 \times 10^{-6} \mu\text{A m}^{-2}$ is white. Magnetic field lines and pressure contours are shown. The central region corresponding to the interior of the star has been artificially blacked out.

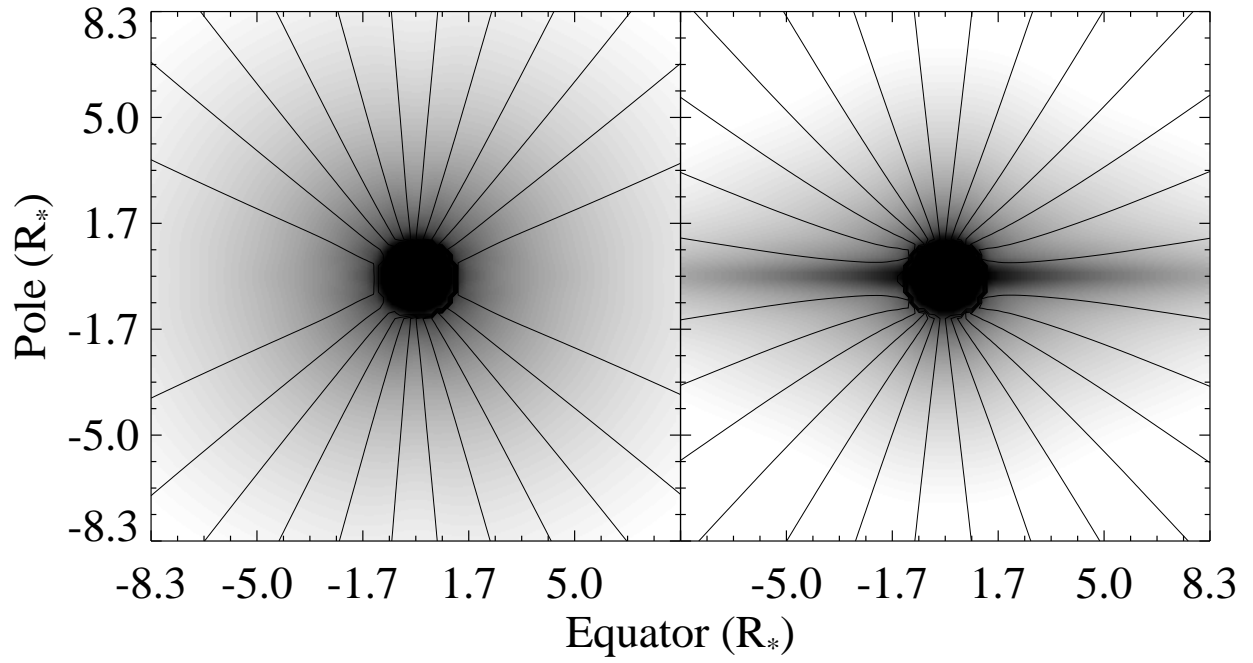


Fig. 4.— A grey-scale image of $\log n$ with magnetic field lines overplotted is shown for the $\beta = 5.0$ (left) and $\beta = 0.1$ (right) cases in steady-state. Only the inner 100×100 grid points are shown. White corresponds to $n \leq 10^{10} \text{ cm}^{-3}$ while $n \geq 10^{11.5} \text{ cm}^{-3}$ is black. The line spacing is proportional to field strength.

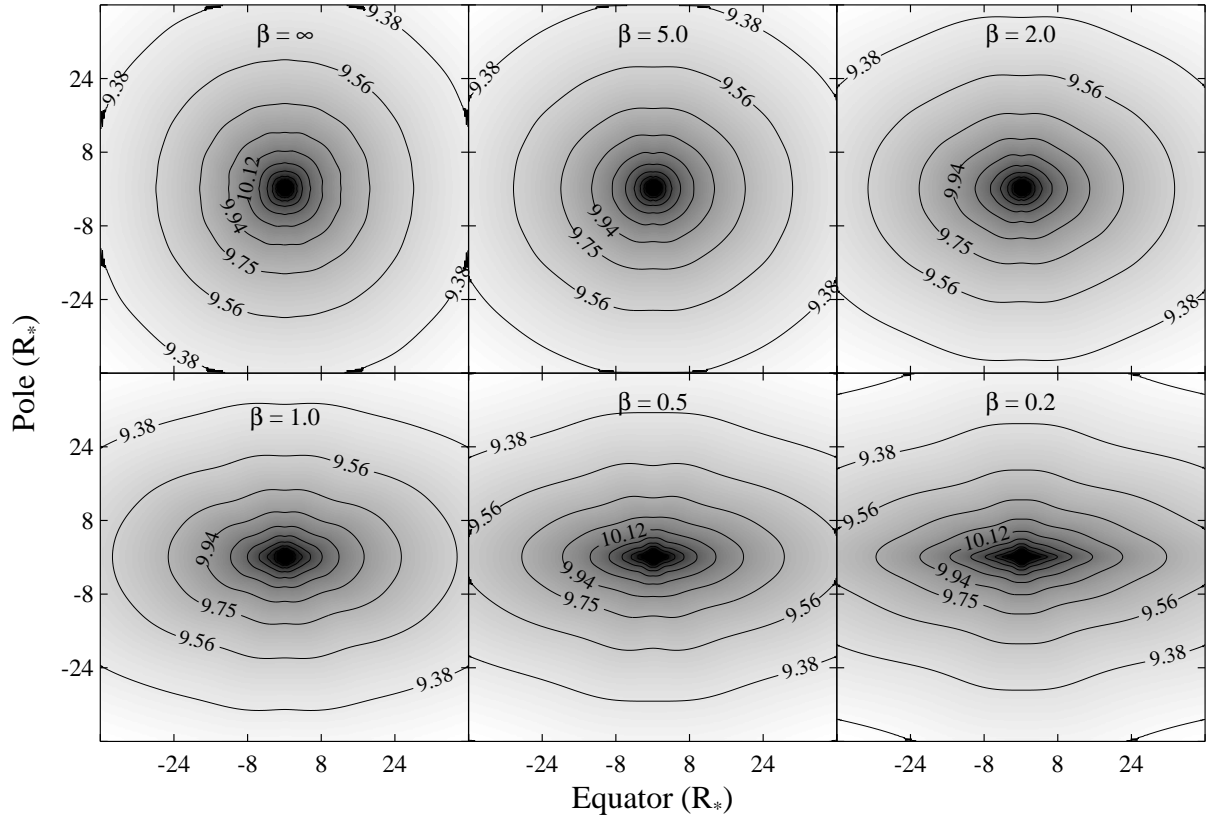


Fig. 5.— Maps of $\log n$ (cm^{-3} , grey-scale and contours) for various cases reveal a relationship between the magnetic field strength and the density distribution of the wind. The value of β is indicated at the top of each panel, and the entire simulation region is shown in its steady-state configuration.

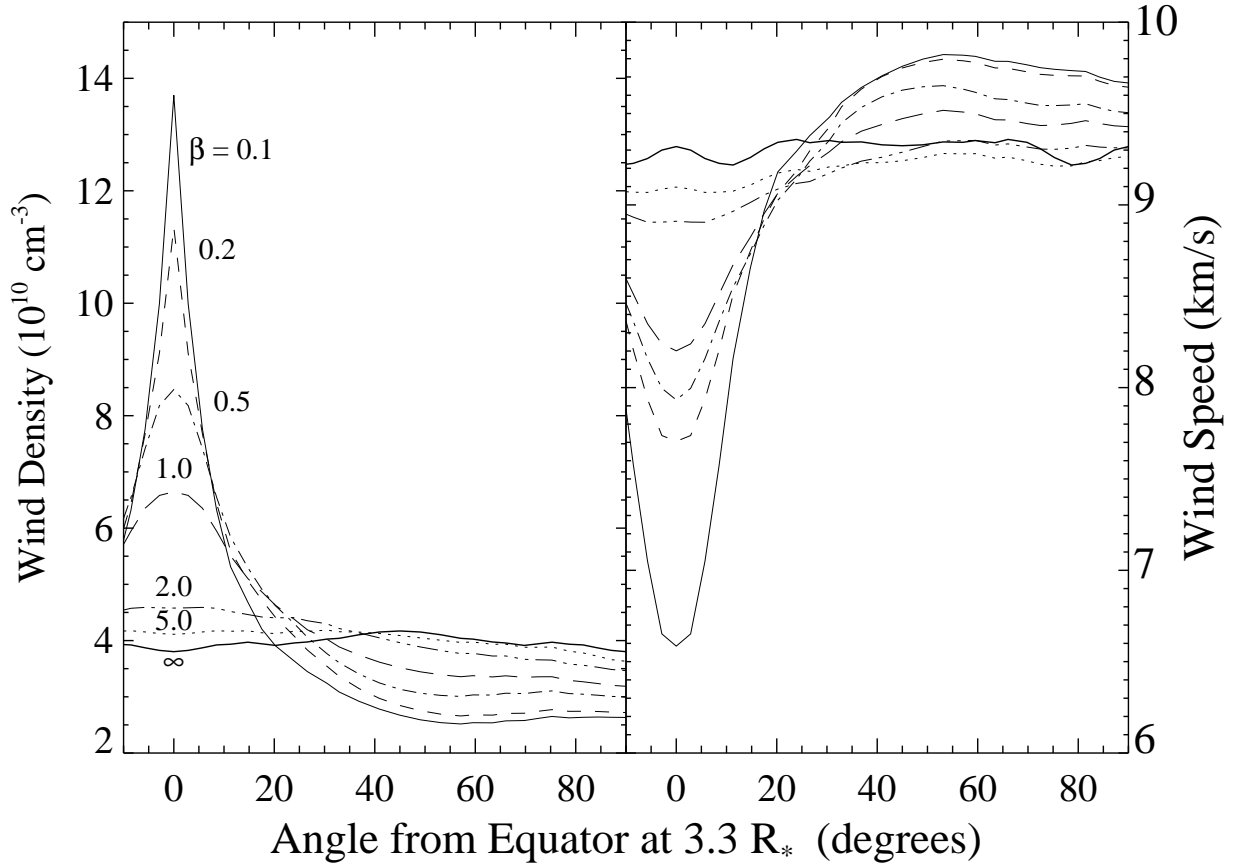


Fig. 6.— Shown is the density (left panel) and wind speed (right panel) at $3.3R_*$ as a function of angle from the magnetic equator for all seven cases. In the left panel, the value of β is indicated next to the peak density of each case. In the right panel, each line style corresponds to the same case as indicated in the left panel.

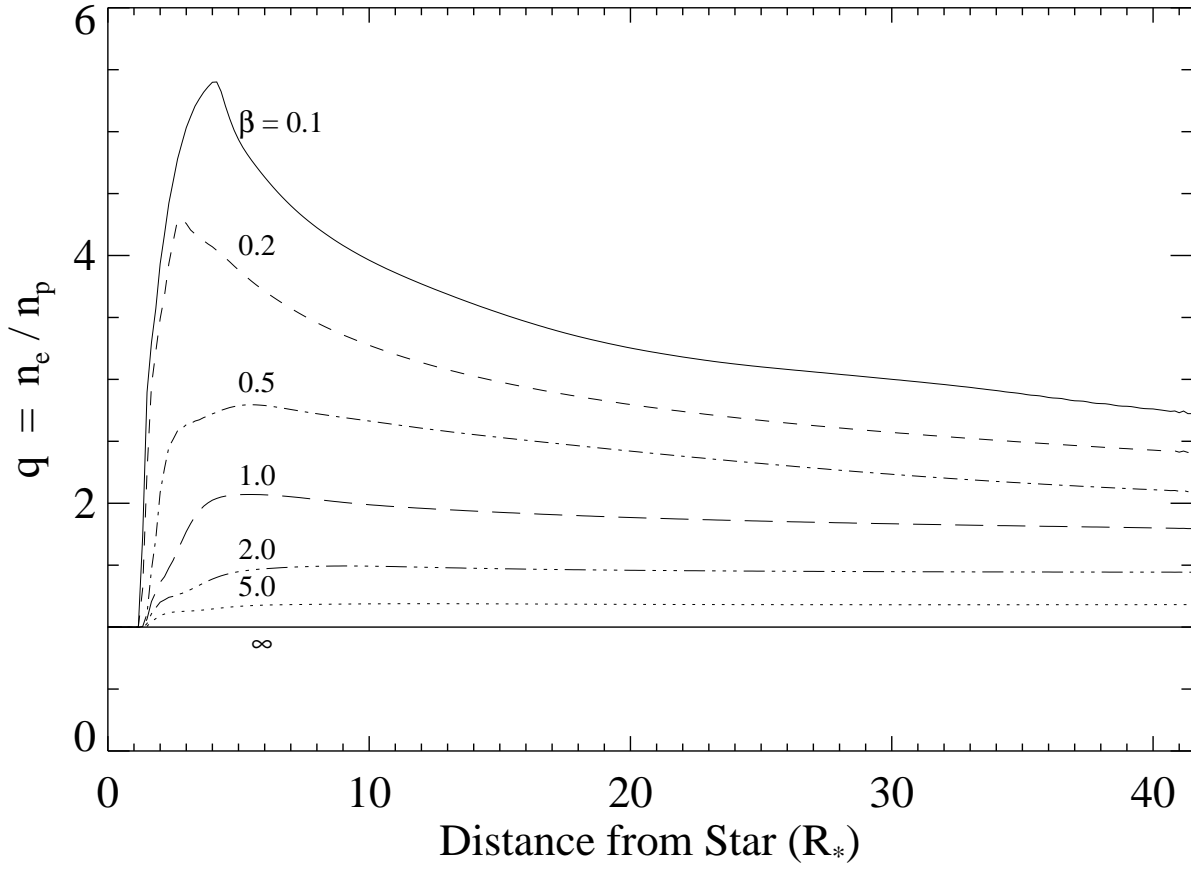


Fig. 7.— The equator-to-pole density contrast, q , is shown as a function of distance from the star for all cases. The value of β is indicated next to the maximum q of each case.

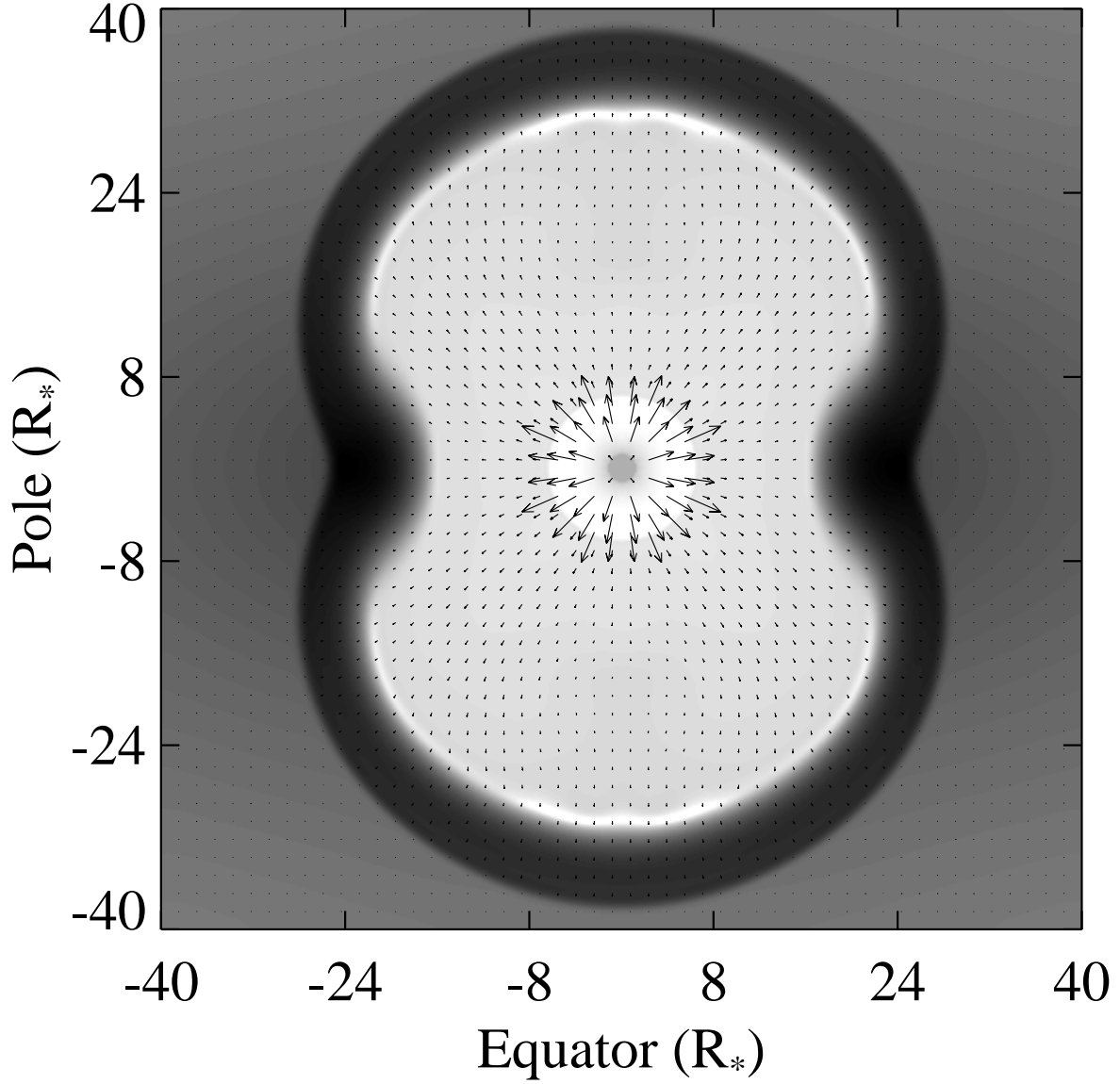


Fig. 8.— An isotropic fast wind collides with an axisymmetric slow wind. The slow wind was produced by the mechanism discussed in the text using a 2.7 Gauss ($\beta = 0.5$) dipole field. Shown is $\log n$ (cm^{-3}) grey-scale with $n \leq 10^{7.5}$ as white and $n \geq 10^{11}$ as black. Also shown are velocity vectors with the maximum length corresponding to 1200 km s^{-1} .